Phytomedicine 23 (2016) 517–527

Contents lists available at ScienceDirect

Phytomedicine

journal homepage: www.elsevier.com/locate/phymed

Preclinical effects of honokiol on treating glioblastoma multiforme via G1 phase arrest and cell apoptosis

Chien-Ju Lin[a], Ya-An Chang[a], Yi-Ling Lin[b], Shing Hwa Liu[c], Cheng-Kuei Chang[d], Ruei-Ming Chen[a,b,e,*]

[a] Comprehensive Cancer Center and Graduate Institute of Medical Sciences, Taipei Medical University, Taipei, Taiwan
[b] Brain Research Center, Wan-Fang Hospital, Taipei Medical University, Taipei, Taiwan
[c] Institute of Toxicology, College of Medicine, National Taiwan University, Taipei, Taiwan
[d] Department of Neurosurgery, Shuang-Ho Hospital, Taipei Medical University Wan-Fang Hospital, Taipei, Taiwan
[e] Anesthetics and Toxicology Research Center, Taipei Medical University Hospital, Taipei, Taiwan

ARTICLE INFO

Article history:
Received 3 December 2015
Revised 17 February 2016
Accepted 23 February 2016

Keywords:
Honokiol
Malignant glioma
p53/CD1/CDKs/E2F1
Cell cycle arrest
Apoptosis

ABSTRACT

Background: Our previous study showed that honokiol, a bioactive polyphenol, can traverse the blood–brain barrier and kills neuroblastoma cells.
Purpose: In this study, we further evaluated the preclinical effects of honokiol on development of malignant glioma and the possible mechanisms.
Methods: Effects of honokiol on viability, caspase activities, apoptosis, and cell cycle arrest in human glioma U87 MG or U373MG cells were assayed. As to the mechanisms, levels of inactive or phosphorylated (p) p53, p21, CDK6, CDK4, cyclin D1, and E2F1 were immunodetected. Pifithrin-α (PFN-α), a p53 inhibitor, was pretreated into the cells. Finally, our *in vitro* findings were confirmed using intracranial nude mice implanted with U87 MG cells.
Results: Exposure of human U87 MG glioma cells to honokiol decreased the cell viability. In parallel, honokiol induced activations of caspase-8, -9, and -3, apoptosis, and G1 cell cycle arrest. Treatment of U87 MG cells with honokiol increased p53 phosphorylation and p21 levels. Honokiol provoked signal-transducing downregulation of CDK6, CDK4, cyclin D1, phosphorylated (p)RB, and E2F1. Pretreatment of U87 MG cells with PFN-α significantly reversed honokiol-induced p53 phosphorylation and p21 augmentation. Honokiol-induced alterations in levels of CDK6, CDK4, cyclin D1, p-RB, and E2F1 were attenuated by PFN-α. Furthermore, honokiol could induce apoptotic insults to human U373MG glioma cells. In our *in vivo* model, administration of honokiol prolonged the survival rate of nude mice implanted with U87 MG cells and induced caspase-3 activation and chronological changes in p53, p21, CDK6, CDK4, cyclin D1, p-RB, and E2F1.
Conclusions: Honokiol can repress human glioma growth by inducing apoptosis and cell cycle arrest in tumor cells though activating a p53/cyclin D1/CDK6/CDK4/E2F1-dependent pathway. Our results suggest the potential of honokiol in therapies for human malignant gliomas.

Introduction

Malignant gliomas are the most common and aggressive primary brain tumors (Cheng et al. 2012). According to the World Health Organization grading system, glioblastoma multiforme (GBM) is considered high-grade (grade IV) gliomas. Because GBM cells are highly mobile and invasive, GBM patients have poor prognoses and high mortality rates (Gunther et al. 2003). Traditionally, the recommended treatment of GBM patients is surgical resection followed by irradiation and adjuvant chemotherapy (Stupp et al. 2005). However, median overall survival rates of GBM patients are 10.2 ~ 14.6 months. The 5-year survival rate of GBM

Abbreviations: ANOVA, analysis of variance; BBB, blood–brain barrier; CDK, cyclin/cyclin-dependent kinase; DAB, 3, 3′-diaminobenzidine; DMSO, dimethyl sulfoxide; FBS, fetal bovine serum; GBM, glioblastoma multiforme; HEPES, 4-(2-hydroxyethyl)-1-piperazineethanesulfonic acid; IC_{50}, half maximal inhibitory concentration; MEM, minimum essential medium; MTT, 3-(4,5-dimethylthiazol-2-yl)-2,5-diphenyltetrazolium bromide; PI, propidium iodide; PAGE, polyacrylamide gel electrophoresis; PBS, phosphate-buffered saline; PFN-α, pifithrin-α; PPAR, peroxisome proliferator-activated receptor; RB, retinoblastoma; SDS, sodium dodecylsulfate.

* Corresponding author at: Graduate Institute of Medical Sciences, Taipei Medical University, 250 Wu-Xing St., Taipei 110, Taiwan. Tel.: +886 2 27361661x3222; fax: +886 2 86621119.
E-mail address: rmchen@tmu.edu.tw (R.-M. Chen).

http://dx.doi.org/10.1016/j.phymed.2016.02.021
0944-7113/

is only 5% (Curtin et al. 2009). The poor outcomes may be due to uncontrolled tumor proliferation, infiltrative growth, angiogenesis, and resistance to apoptosis (Staudacher et al. 2014). Therefore, treating malignant gliomas remains a challenge. Discovering more-effective therapeutic agents for brain cancer therapy is an urgent issue.

Chinese herbal medicine is a common alternative therapy for cancer patients in Asian and Western countries (Liu et al. 2012). Some natural active compounds isolated from Chinese medicinal herbs were proven to possess anticancer effects against a variety of tumors (Tan et al. 2011). Honokiol, a bioactive polyphenol extracted from the traditional Chinese medicine, Houpo, exhibits diverse pharmacological effects, including anti-inflammatory, antimicrobial, antithrombotic, and anxiolytic effects (Hahm and Singh 2007; Park et al. 2009). As to the mechanisms, honokiol has antitumor activities against leukemia, breast cancer, pancreatic cancer, and oral squamous cell carcinoma cells due to induction of cell cycle arrest and cell apoptosis (Ishikawa et al. 2012). In addition, honokiol can inhibit the invasion and migration of breast cancer cells (Nagalingam et al. 2012). Our previous study further demonstrated that honokiol can traverse the blood-brain barrier (BBB) and induces apoptotic insults to neuroblastoma cells (Lin et al. 2012). However, little is known as to whether honokiol has antitumor consequences against GBM.

Progression of cell cycle is controlled by a series of events, including cyclin/cyclin-dependent kinase (CDK) complexes and their inhibitors (Becker and Bonni 2004). Complexes of activated cyclin D and CDK4/6 can cause phosphorylation of the retinoblastoma (RB) protein. E2F, a transcription factor, can promote cell cycle progression from the G_1 to S phase (Becker and Bonni 2004; Niehrs and Acebron 2012). The RB protein interacts with E2F and lessens its transcriptional activity. Nevertheless, the phosphorylated (p)-RB protein releases E2F to induce E2F-target gene expressions that are required for regulating the cell cycle (Becker and Bonni 2004). In response to a range of stimuli, p53, a tumor suppressor protein, is phosphorylated and activated in cancer cells (Polager and Ginsberg, 2009). Activated p53 regulates tumor cell activities through inducing cell cycle arrest, cell senescence, cell differentiation, and cell apoptosis mediated by the CDK inhibitor, p21 (Polager and Ginsberg, 2009). Thus, exploring p53-involved signaling pathway would be helpful in discovering new drugs for treating malignant gliomas. In this study, we investigated the effects of honokiol on killing U87 MG glioma cells and its possible molecular mechanisms. Additionally, our *in vitro* findings were further confirmed using an intracranial glioma animal model.

Materials and methods

Cell culture and drug treatment

The human glioma U87 MG and U373MG cell lines were purchased from American Type Culture Collection (Manassas, VA, USA). Cells were maintained in Minimum Essential Medium (Gibco-BRL, Grand Island, NY, USA) supplemented with 10% fetal bovine serum, 2 mM L-glutamine, 100 IU/ml penicillin, 100 mg/ml streptomycin, 1 mM sodium pyruvate, and 1 mM nonessential amino acids at 37 °C in a humidified atmosphere of 5% CO_2. Cells were grown to confluence before drug treatment. Honokiol was purchased from Sigma (St. Louis, MO, USA) and freshly dissolved in dimethyl sulfoxide (DMSO). The purity of honokiol used in this study is more than 98%. Cells were exposed to different concentrations of honokiol for various time intervals.

Cell viability assay

Cell viability was assayed using a colorimetric method. U87 MG cells (8×10^3 cells/well) were seeded on a 96-well plate for 24 h and then exposed to honokiol. Before the end of treatment, 0.5 mg/ml 3-(4,5-dimethylthiazol-2-yl)-2,5-diphenyltetrazolium bromide was added to each well for 4 h. Supernatants were carefully aspirated, and formazan crystals were dissolved in DMSO. Absorbance was measured at 550 nm with a microplate reader (Biochrom, Holliston, MA, USA).

Cell cycle analysis

U87 MG cells were seeded on 6-well plates for 24 h. After individual treatments, whole cells were collected and centrifuged. Pellets were re-suspended in phosphate-buffered saline (PBS) and fixed in ice-cold 70% ethanol. Cells were then washed with PBS and incubated in PBS containing 0.5 mg/ml RNase A and 40 mg/ml propidium iodide (PI) at 37 °C for 30 min. The cell cycle was analyzed by flow cytometry (Beckman Coulter, Brea, CA, USA). Results were further analyzed using software (Beckman Coulter).

Quantification of apoptotic and necrotic cells

The mode of cell death was analyzed by flow cytometry with annexin V/PI double-staining to detect membrane events according to a previous study (Pietra et al. 2001). After individual treatments, whole cells were collected in 4-(2-hydroxyethyl)-1-piperazineethanesulfonic acid (HEPES) buffer containing 10 mM HEPES (pH 7.4), 140 mM NaCl, and 2.5 mM $CaCl_2$. Cells were subsequently stained with annexin V and PI for 20 min, followed by analysis by flow cytometry (Beckman Coulter). Cytograms of the four quadrants in the figure were used to distinguish normal (annexin V^-/PI^-), early apoptotic (annexin V^+/PI^-), late apoptotic (annexin V^+/PI^+), and necrotic cells (annexin V^-/PI^+). The sum of early apoptosis and late apoptosis is presented as total apoptosis.

Assay of caspase activities

Activities of caspase-8 and -9 were assayed using fluorometric assay kits (R&D Systems, Minneapolis, MN) as described previously (Chen et al. 2013). The peptide substrates for assays of caspase-8 and -9 activities were Ile-Glu-Thr-Asp (IETD) and Leu-Glu-His-Asp (LEHD), respectively.

Immunoblotting analyses

After drug treatment, U87 MG cells were washed with PBS and lysed with ice-cold lysis buffer (25 mM HEPES, 1.5% Triton X-100, 0.1% sodium dodecylsulfate (SDS), 0.5 M NaCl, 5 mM EDTA, and 0.1 mM sodium deoxycholate) containing a protease inhibitor cocktail. Protein concentrations were quantified using a bicinchoninic acid protein assay kit (Thermo, San Jose, CA, USA). An equal amount of proteins from each group was separated using SDS-polyacrylamide gel electrophoresis (PAGE), followed by transfer to nitrocellulose membranes. Membranes were incubated with a 5% skim milk solution for 1 h, and then incubated with indicated antibodies at 4 °C for 16 h. Membranes were probed with the appropriate horseradish peroxidase-conjugated secondary antibodies for 1 h at room temperature. Immunoreactive proteins were detected using an enhanced chemiluminescence reagent (PerkinElmer, Waltham MA, USA) and then imaged using a digital analyzer (Syngene, Cambridge, UK) and a densitometry software (Syngene). Anti-CDK6, CDK4, cyclin D1, E2F1, p53, and *p21* antibodies were purchased from Santa Cruz Biotechnology (Santa Cruz, CA, USA). Anti-p-pRB, p-p53, and caspase-3 antibodies were purchased from Cell Signaling Technology (Beverly, MA, USA). The anti-RB antibody was purchased from GeneTex (Irvine, CA, USA). The cellular β-actin protein was immunodetected using a mouse monoclonal antibody (Sigma) as the internal standard. The density of bands was determined with an analyzer (Syngene).

Animal brain tumor model

All experimental procedures were performed according to the National Institutes of Health *Guidelines for the Use of Laboratory Animals* and approved by the Institutional Animal Care and Use Committee of Taipei Medical University (Taipei, Taiwan). Six-week-old female BALB/c *nu*/*nu* mice were purchased from the National Laboratory Animal Center (Taipei, Taiwan), housed in a sterile environment, and allowed free access to food and water. Animals were anesthetized by inhalation of isoflurane and then were stereotactically inoculated with 2×10^5 U87 MG cells into the right frontal lobe using a Hamilton syringe (Reno, NV, USA) and a syringe pump (SINGA Technology Corporation, Taipei, Taiwan). Intracranial glioma-bearing mice were randomly divided into two groups ($n = 5$/group) 4 days after tumor implantation and then intraperitoneally injected with 20 mg/kg honokiol or vehicle (10% DMSO in PBS) two times per week for 2 weeks according to a method previously (Wang et al. 2011). At the end of the experiments, a Kaplan-Meier survival analysis was performed. For immunoblotting analyses, the brains were collected and homogenized with the RIPA buffer. After centrifugation, the supernatants were collected. Protein concentrations were quantified using a bicinchoninic acid protein assay kit (Thermo). An equal amount of proteins from each group was separated using SDS-PAGE and then transferred to nitrocellulose membranes. After blocking, the membranes were incubated with indicated antibodies. These immunoreactive protein bands were detected using an enhanced chemiluminescence reagent (PerkinElmer) and then analyzed by a digital analyzer (Syngene).

Immunohistochemistry

After drug administration, the animals were sacrificed and brains were collected for immunohistochemical analysis of cleaved caspase-3. Briefly, brain tissues were fixed in 4% paraformaldehyde in PBS, embedded in paraffin, and sectioned. Sections were deparaffinized with xylene, rehydrated with a graded alcohol series, followed by antigen target retrieval for 20 min. Endogenous peroxidase activity was quenched in a 3% H_2O_2 solution. Slides were incubated in blocking solution (Vector Laboratories, Burlingame, CA, USA) for 1 h. Primary antibodies for cleaved caspase-3 were incubated at 4 °C overnight followed by incubation with biotin-conjugated secondary antibodies, for 1 h at room temperature. Slides were subsequently detected using a Vectastain ABC kit (Vector Laboratories). 3, 3′-Diaminobenzidine (DAB, Vector Laboratories) is a substrate for peroxidase. Sections were counterstained with hematoxylin, followed by dehydration in a graded alcohol series and xylene, with the addition of a coverslip. Photomicrographs were taken at 200x magnification with a Nikon microscope equipped with a digital camera (Nikon, Melville, NY).

Statistical analysis

The statistical significance of differences between control and drug-treated groups was evaluated using Student's *t*-test, and differences were considered statistically significant at $p < 0.05$. Differences between drug-treated groups were considered significant when the p value of Duncan's multiple-range test was < 0.05. Statistical analyses between groups over time were carried out by a two-way analysis of variance (ANOVA). The survival rate of tumor-bearing mice was examined using a log-rank test. A p value of < 0.05 was considered statistically significant.

Results

Honokiol decreases the viability of human glioma U87 MG cells via inducing cell apoptosis. Treatment of U87 MG cells with 10 μM honokiol for 72 h did not affect cell viability (Fig. 1A). When the administered concentrations reached 20, 40, 80, and 100 μM, honokiol caused significant 23%, 34%, 83%, and 91% decreases in cell viability, respectively. The half maximal inhibitory concentration (IC_{50}) of honokiol was 52.7 μM. In addition, exposure of U87 MG cells to 40 μM honokiol for 24, 48 and 72 h reduced cell viability by 18%, 31% and 42% (Fig. 1B). In parallel, honokiol at 10 μM did not induce apoptosis of U87 MG cells (Fig. 1C). However, exposure to 20, 40, 80, and 100 μM honokiol induced 5%, 33%, 60%, and 77% cell apoptosis, respectively. In contrast, honokiol did not trigger cell necrosis (Fig. 1C). Treatment of U87 MG cells with 40 μM honokiol for 48 and 72 h respectively induced 16% and 32% cell apoptosis without influencing cell necrosis (Fig. 1D). Additionally, exposure of U87 MG cells to 40 μM honokiol for 12 and 24 h did not alter levels of pro- and cleaved caspase-3 (Fig. 1E, top two panels, lanes 2 and 3). Following exposure for 48 and 72 h, honokiol decreased cellular pro-caspase-3 amounts but increased cleaved caspase-3 levels (lanes 4 and 5). When treated with honokiol for 48 and 72 h, levels of pro-caspase-3 decreased by 38% and 55%, respectively. Meanwhile, amounts of cleaved caspase-3 were obviously augmented (Fig. 1F). Exposure of U87 MG cells to 40 μM honokiol for 72 h led to significant 71% and 174% increases in activities of caspase-8 and -9, respectively (Table 1).

Table 1
Effects of honokiol on activities of caspase-8 and -9 in human U87 MG glioma cells.

	Control	Honokiol
Caspase-8 activity (fluorescent intensities)	34 ± 6	58 ± 7*
Caspase-9 activity (fluorescent intensities)	43 ± 9	118 ± 25*

Human U87 MG cells were exposed to 40 μM honokiol for 72 h. Activities of caspase-8 and -9 were determined using fluorometric methods. Each value represents the mean ± SEM from three independent experiments. * Values significantly differ from the respective control, $p < 0.05$.

Honokiol induces cell cycle arrest and stimulates p53-dependent signals in human glioma cells. Treatment of U87 MG cells with 40 μM honokiol for 24 h did not affect the sub-G_1 phase (Fig. 2A). However, exposure to honokiol for 48 and 72 h caused 3.6- and 7-fold increases in proportions of cells in the sub-G_1 phase. In comparison, treatment with honokiol for 24 ~ 72 h enhanced the proportions of U87 MG cells in the G_1 phase in a time-dependent manner (Fig. 2A). In parallel, proportions of cells in the S and G_2/M phases decreased following honokiol treatment. Furthermore, exposure of U87 MG cells to 40 μM honokiol for 12 ~ 72 h increased levels of p-p53 and p53 (Fig. 2B, top two panels) After exposure of U87 MG glioma cells to 40 μM honokiol for 24, 48, and 72 h, levels of p-p53 were significantly elevated by 1.7-, 2.9-, and 3.3-fold, respectively (Fig. 2C, black columns). Amounts of p53 were also augmented by 2.1-, 2.6-, 2.3-, and 1.4-fold after U87 MG cells were treated with honokiol for 12, 24, 48, and 72 h, respectively (Fig. 2C, white columns). Meanwhile, levels of p21 increased (Fig. 2D, top panel). When treated for 12, 24, 48, and 72 h, honokiol caused 1.8-, 2.7-, 3.7-, and 3.3-fold increases in the amounts of p21, respectively (Fig. 2E).

Honokiol affects cell cycle checkpoint proteins in glioma cells. Exposure of U87 MG cells to 40 μM honokiol decreased levels of CDK6 and CDK4 (Fig. 3A, top two panels). When treated with honokiol for 12, 24, 48, and 72 h, levels of CDK6 decreased 0.68-, 0.62-, 0.47-, and 0.56-fold, respectively (Fig. 3B, black columns). Meanwhile, amounts of CDK4 were suppressed to 0.75-, 0.48-, 0.49-, and 0.28-fold (white columns). In parallel, levels of cyclin D1 also decreased due to honokiol (Fig. 3C, top panel). Exposure of U87 MG cells to 40 μM honokiol for 12, 24, and 48 h decreased the level of cyclin D to 0.32-fold. Following exposure for 72 h, the level of cyclin D significantly dropped to 0.07-fold (Fig. 3D). Subsequently, treatment of U87 MG cells with 40 μM honokiol for 12 ~ 72 h suppressed the protein level of p-RB (Fig. 3E, first panel, lanes

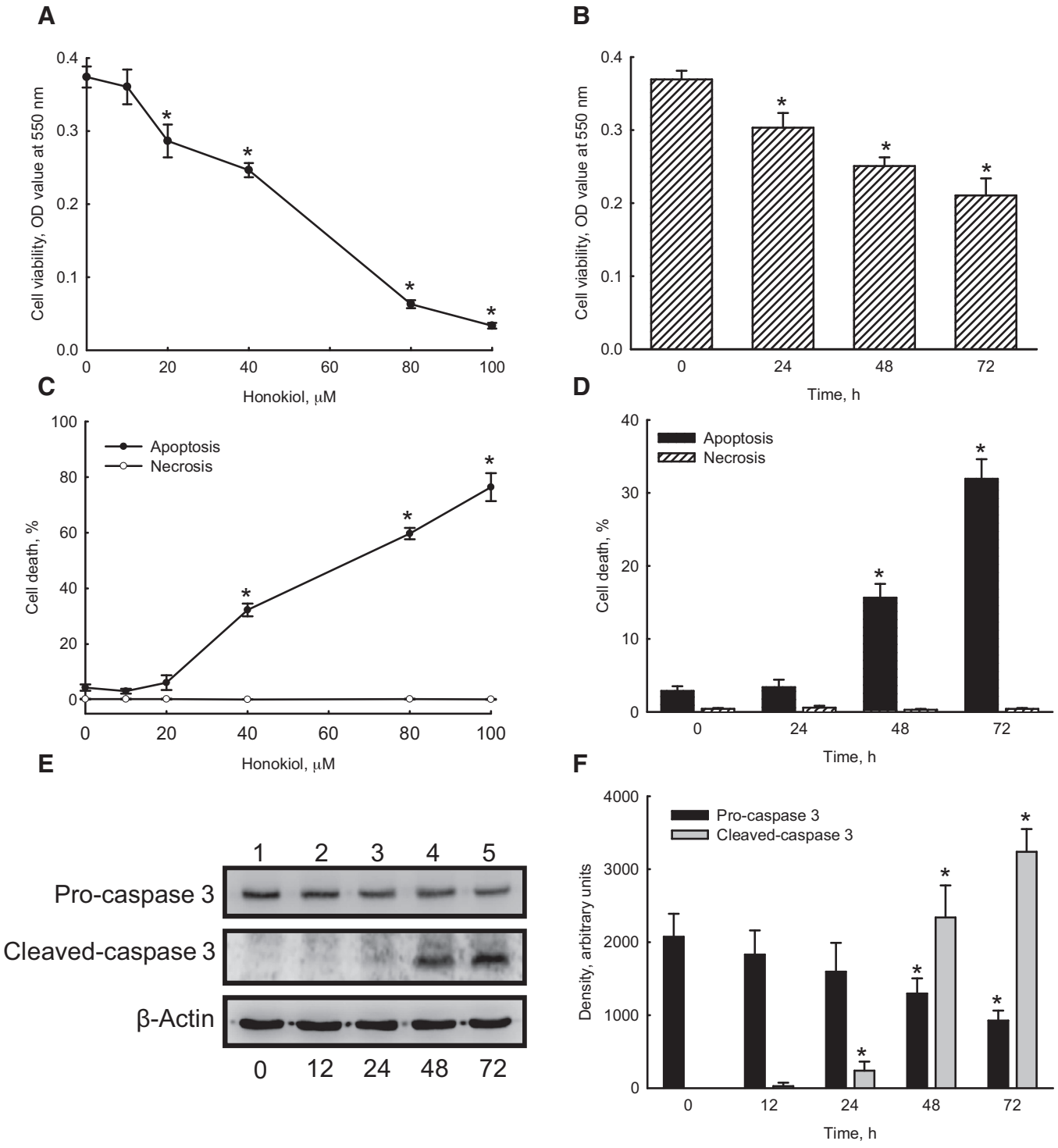

Fig. 1. Effects of honokiol on the viability, necrosis, and apoptosis of human glioma cells. U87 MG cells were exposed to 10, 20, 40, 80, and 100 μM honokiol for 72 h (A, C) or to 40 μM honokiol for 24, 48, and 72 h (B, D–F). Cell viability was assessed using a colorimetric method (A, B). After staining with annexin V/propidium iodide, apoptotic and necrotic cells were quantified using flow cytometry (C, D). Levels of pro- and cleaved caspase-3 were immunodetected (E, top two panels). β-Actin was analyzed as an internal standard (bottom panel). These protein bands were quantified and statistically analyzed (F). Each value represents the mean ± SEM from six independent experiments. Representative immunoblotting images are shown.* Values significantly differ from the respective control, $p < 0.05$.

2 to 5). After exposure of U87 MG cells to 40 μM honokiol for 12, 24, 48, and 72 h, levels of the p-RB protein significantly decreased to 0.54-, 0.41-, 0.34-, and 0.28-fold, respectively (Fig. 3F). Meanwhile, amounts of E2F1 were also suppressed by honokiol (Fig. 3G, top panel). Exposure of U87 MG cells to 40 μM honokiol for 12, 24, 48, and 72 h decreased the level of E2F1 to 0.61-, 0.22-, 0.19-, and 0.35-fold, respectively (Fig. 3H).

Activation of p53 mediates honokiol-induced cell cycle arrest. To further investigate the role of p53 in cell cycle arrest, a p53 inhibitor, cyclic PFN-α, was used in combination with honokiol (Fig. 4). Treatment of U87 MG cells with 10 μM PFN-α alone for 72 h suppressed the protein level of p53, but did not affect the protein level of p-p53 (Fig. 4A, top two panels, lane 2). When U87 MG cells were pretreated with 10 μM PFN-α for 1 h followed by 40 μM

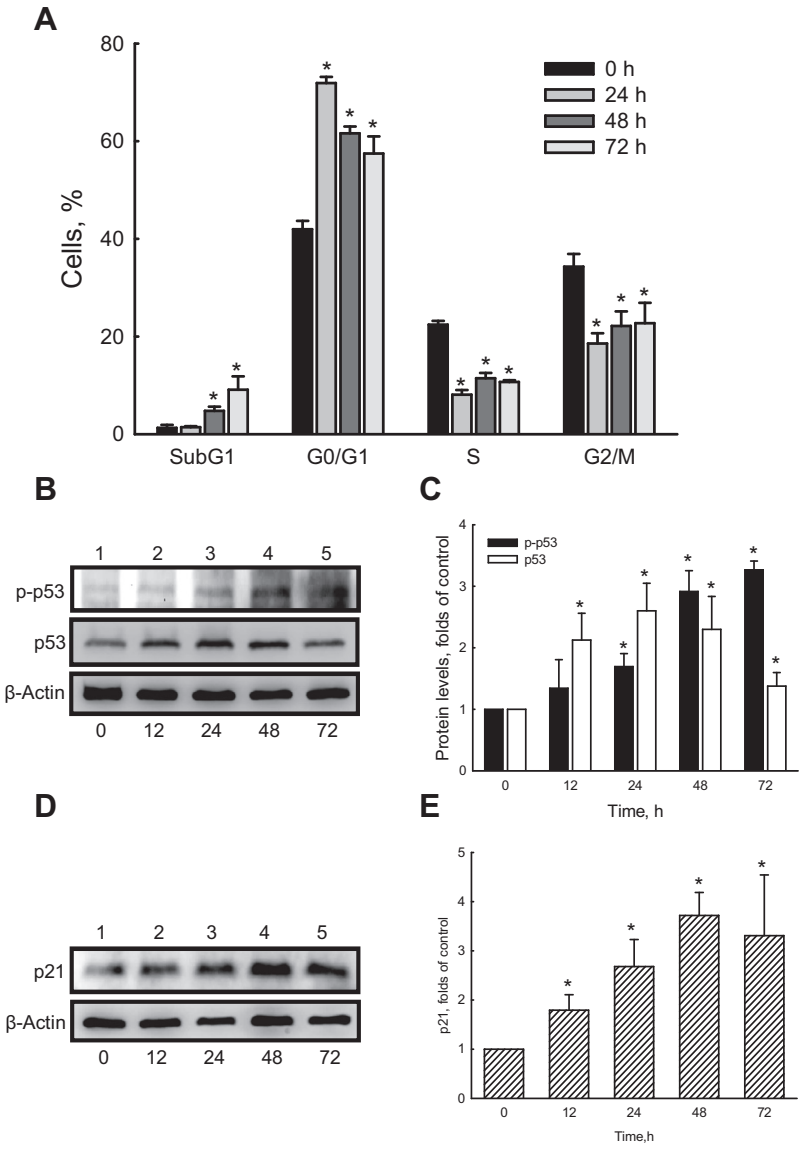

Fig. 2. Effects of honokiol on p53-dependent signals in human glioma cells. (A) U87 MG cells were exposed to 40 μM honokiol for 24, 48, and 72 h. The cell cycle was analyzed by flow cytometry. Cells were exposed to 40 μM honokiol for 12, 24, 48, and 72 h, and levels of p53 and phosphorylated (p)-p53 were immunodetected (B, top two panels). Sequentially, levels of p21 were further analyzed (D, top panel). β-Actin was detected as an internal standard (B, D, bottom panels). These protein bands were quantified and statistically analyzed (C, E). Each value represents the mean ± SEM from three independent experiments. Representative immunoblotting images are shown. * Values significantly differ from the respective control, $p < 0.05$.

honokiol for another 72 h, levels of p-p53 and p53 both decreased (lane 4). Exposure of U87 MG cells to PFN-α and honokiol reduced levels of p-p53 from 2.77- to 0.96-fold (Fig. 4B, black columns), and levels of p53 from 2.44- to 1.00-fold (gray columns). Meanwhile, the honokiol-increased level of p21 was also suppressed by PFN-α (Fig. 4C, top panel, lane 4). After treatment with 10 μM PFN-α and 40 μM honokiol for 72 h, the level of p21 was reduced from 2.92- to 0.62-fold (Fig. 4D). Exposure of U87 MG cells to 10 μM PFN-α did not affect cell cycle phases (Fig. 4E). After U87 MG cells were pretreated with 10 μM PFN-α for 1 h and then 40 μM honokiol for another 72 h, honokiol-induced G_0/G_1 cell cycle arrest was reversed. Proportions of glioma cells arrested in the G_1 phase decreased from 53.1% to 43.4% (Fig. 4E).

p53 regulates cell cycle checkpoint proteins. When U87 MG cells were pretreated with PFN-α for 1 h, honokiol-suppressed protein levels of CDK6 and CDK4 were reversed (Fig. 5A, top two panels, lane 4). Compared to the honokiol alone group, exposure of U87 MG cells to 10 μM PFN-α and 40 μM honokiol increased the level of CDK6 from 0.54- to 0.91-fold (Fig. 5B, black columns) and the level of CDK4 from 0.28- to 0.63-fold (white columns). In parallel, PFN-α also reversed the level of cyclin D1 (Fig. 5C, top panel). PFN-α treatment increased the honokiol-suppressed level of cyclin D1 from 0.25- to 0.98-fold (Fig. 5D). Reduced amounts of the p-RB protein also increased with PFN-α (Fig. 5E, top panel). Compared to the honokiol-treated group, the level of p-RB in the PFN-α and honokiol treatment group increased from 0.40- to 0.77-fold (Fig. 5F). Similarly, the addition of PFN-α increased the E2F1 level (Fig. 5G). Honokiol decreased the level of E2F1 to 0.47-fold, which was reversed to 0.90-fold when combined with PFN-α (Fig. 5H).

Honokiol induces apoptotic insults to human U373MG glioma cells. Exposure of human U373MG cells to honokiol for 72 h caused a significant 48% decrease in cell viability (Table 2). In parallel, honokiol induced apoptosis of human U373MG cells by 38%. However, honokiol did not trigger cell necrosis (Table 2). Sequentially, the activity of caspase-9 in human U373MG cells was augmented by 2.8-fold after treatment with honokiol (Table 2).

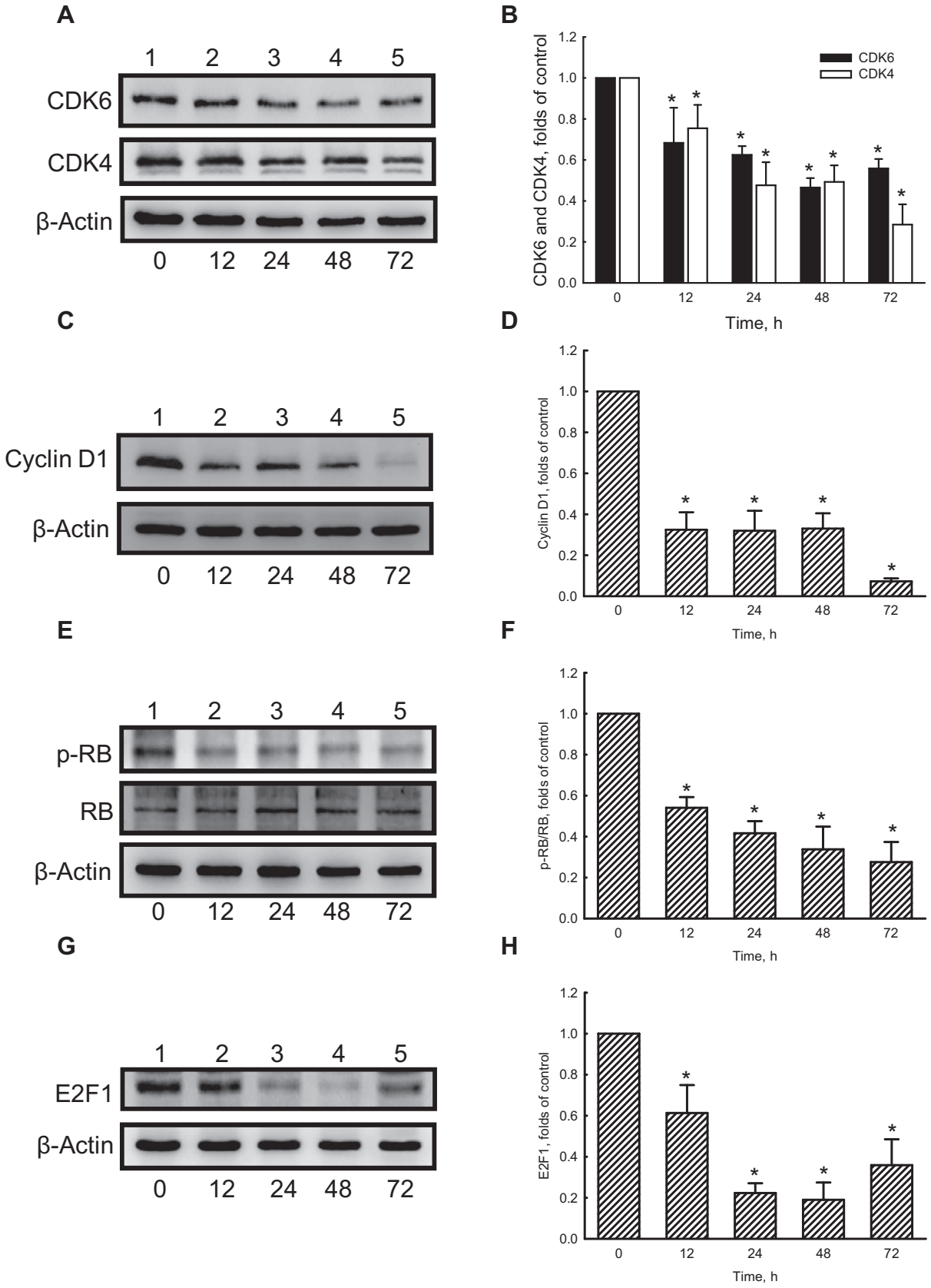

Fig. 3. Effects of honokiol on regulation of cell cycle regulatory proteins in human glioma cells. U87 MG cells were exposed to 40 μM honokiol for 12, 24, 48, and 72 h. Levels of CDK6, CDK4 (A, top two panels), cyclin D1 (C, top panel), p-RB (E, top panel), and E2F1 (G, top panel) were immunodetected. β-Actin (A, C, G, bottom panels) and RB protein (E, second panel) were detected as internal standards. These protein bands were quantified and statistically analyzed (B, D, F, H). Each value represents the mean ± SEM from three independent experiments. Representative immunoblotting images are shown. * Values significantly differ from the respective control, $p < 0.05$.

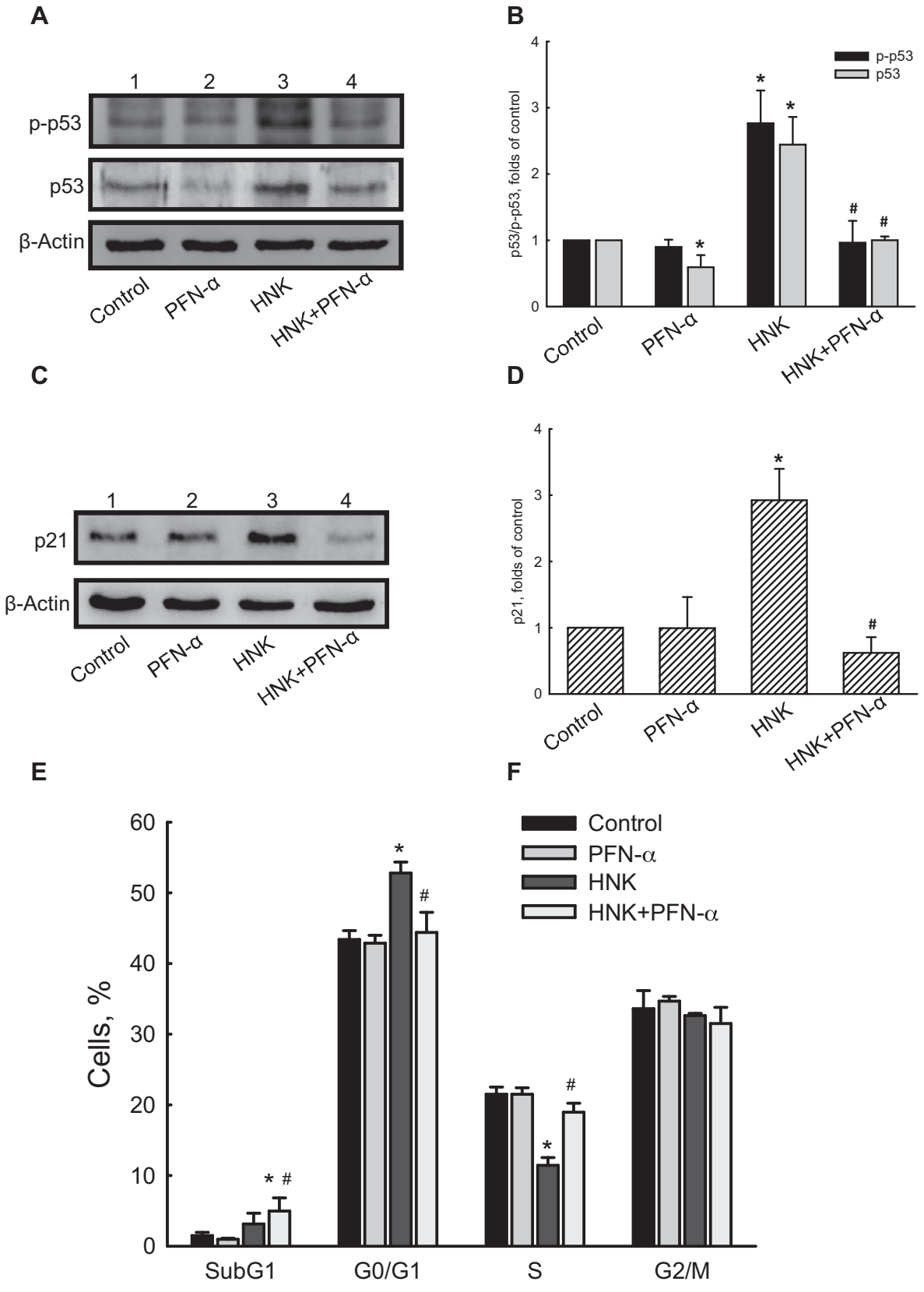

Fig. 4. Effects of pifithrin-α, p-nitro, cyclic (PFN-α) on honokiol (HNK)-altered levels of phosphorylated (p)-p53, p53, and p21, and cell cycle. U87 MG cells were pretreated with 10 μM PFN-α for 1 h, and then exposed to 40 μM HNK for another 72 h. Levels of p-p53 and p53 were immunodetected (A, top two panels). Furthermore, amounts of p21 were analyzed (C, top panel). β-Actin was analyzed as an internal standard (A, C, bottom panels). These protein bands were quantified and statistically analyzed (B, D). (E) The cell cycle was analyzed using flow cytometry. Each value represents the mean $\pm$ SEM from three independent experiments. Representative immunoblotting images are shown. * Values significantly differ from the respective control, $p < 0.05$. # Values significantly differ from the respective honokiol group, $p < 0.05$.

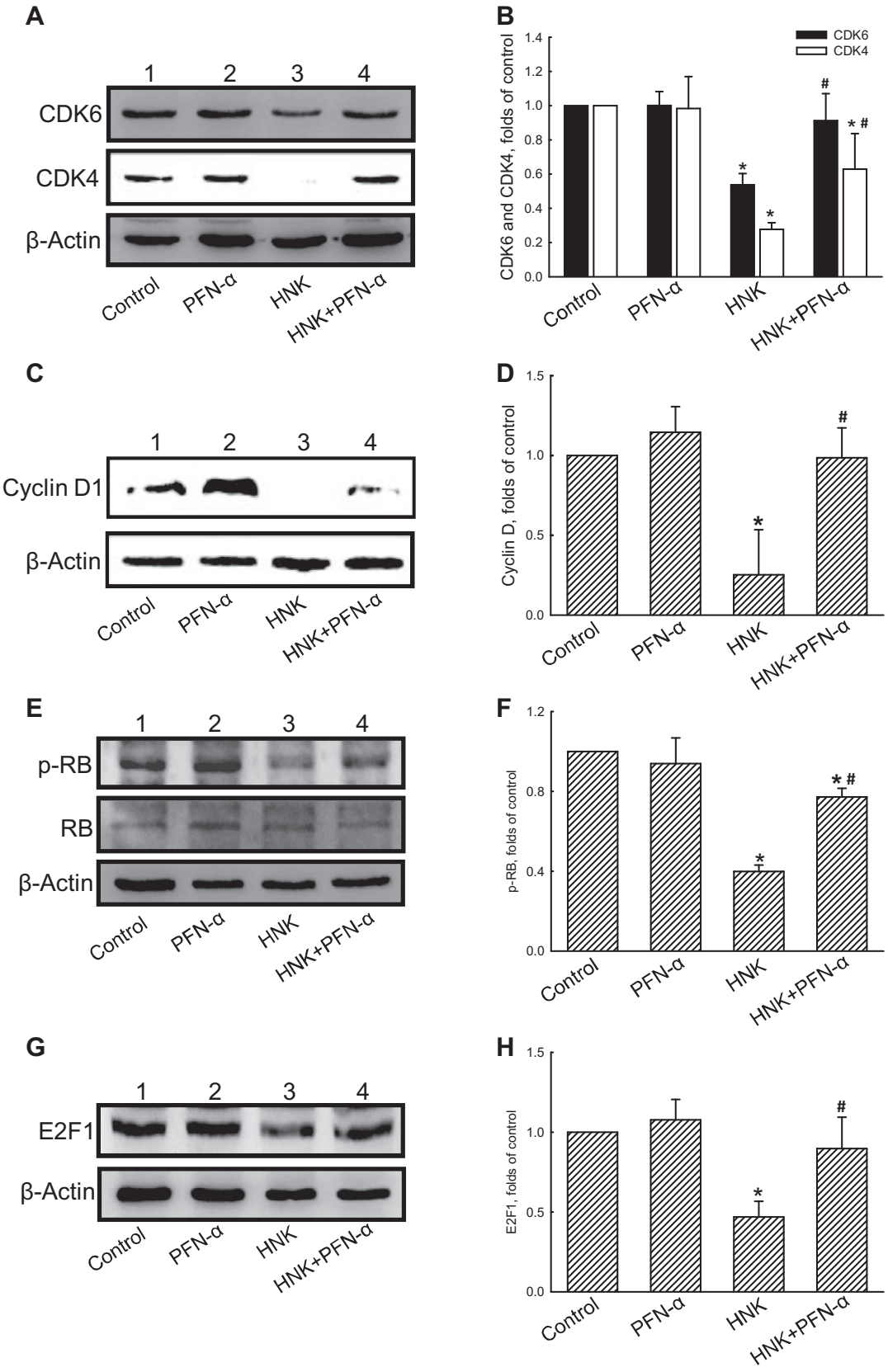

Fig. 5. Effects of pifithrin-α, p-nitro, cyclic (PFN-α) on honokiol-altered levels of cell cycle regulatory proteins. U87 MG cells were pretreated with 10 μM PFN-α for 1 h, and then exposed to 40 μM honokiol (HNK) for another 72 h. Levels of CDK6, CDK4, (A, top two panels), cyclin D1 (C, top panel), the phosphorylated (p)-retinoblastoma (RB) protein (E, top panel), and E2F1 (G, top panel) were immunodetected. β-Actin (A, C, G, bottom panels) and the RB protein (E, bottom panel) were analyzed as internal standards. These protein bands were quantified and statistically analyzed (B, D, F, H). Each value represents the mean ± SEM from three independent experiments. Representative immunoblotting images are shown. * Values significantly differ from the respective control, $p < 0.05$. # Values significantly differ from the respective honokiol group, $p < 0.05$.

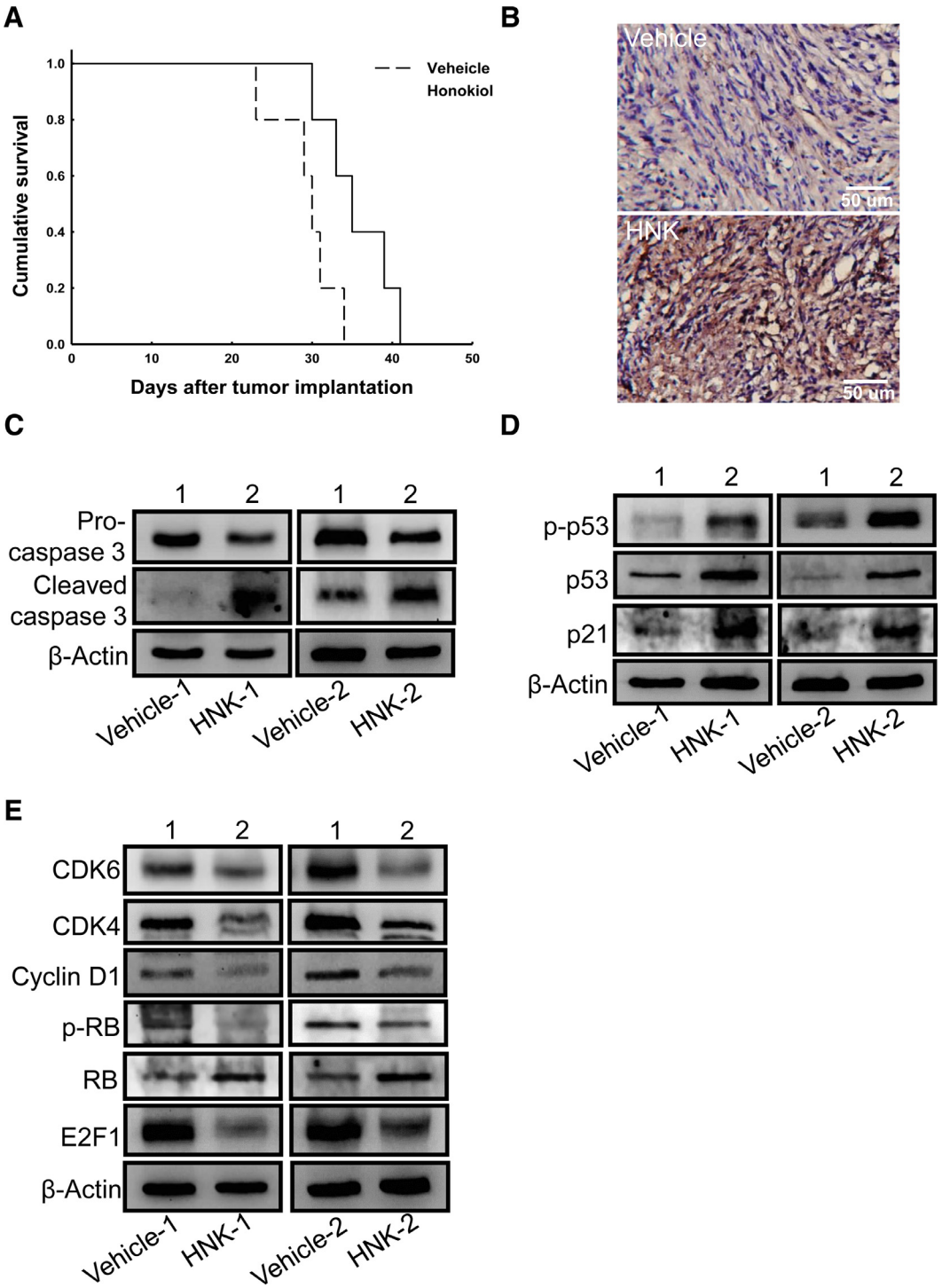

Fig. 6. Efficacy of honokiol (HNK) on survival rates of mice bearing gliomas and the related mechanisms. U87 MG cells were intracranially implanted into brains of nude mice. On day 4 after U87 MG inoculation, nude mice ($n = 5$ in each group) were treated with HNK as described in "Materials and methods". A, Kaplan–Meier survival curve was analyzed by a log-rank test ($p < 0.05$). After sacrifice, the brains were collected for immunohistochemical analyses or homogenized for protein assays. Immunohistological analyses of cleaved caspase-3 were carried out (B). Levels of pro- and cleaved caspase-3 (C, top two panels), phosphorylated (p)-p53, p53, and p21 (D, top three panels), and CDK6, CDK4, cyclin D1, p-retinoblastoma (RB) protein, and E2F1 (E, top four and 6th panels) were immunodetected. β-Actin and RB (B–D) were detected as internal standards. Two representative protein blots are shown from this study.

In vivo efficacy of honokiol in mice with intracranial gliomas. The antitumor efficacy of honokiol was also evaluated in an animal brain tumor model (Fig. 6). At the end of the experiment, the survival rate of mice was analyzed. Median survival times of mice treated with vehicle and honokiol were 30 and 36 days, respectively (Fig. 6A). Honokiol treatment significantly increased the survival rate of mice ($P < 0.01$). As to the mechanisms, immunohistochemical analysis showed that low levels of cleaved caspase-3 in vehicle-treated brain tumors (Fig. 6B). In contrast, administration of honokiol enhanced amounts of cleaved caspase-3

Table 2
Effects of honokiol on insults to human U373MG glioma cells.

	Control	Honokiol
Cell Viability (OD value at 550 nm)	0.401 ± 0.035	0.209 ± 0.021*
Apoptotic cells (%)	4 ± 1	38 ± 6*
Necrotic cells (%)	3 ± 1	4 ± 1
Caspase-9 activity (fluorescent intensities)	38 ± 6	105 ± 17*

Human U373MG glioma cells were exposed to 40 μM honokiol for 72 h. Cell viability was assessed using a colorimetric method. Apoptotic and necrotic cells were quantified using flow cytometry. Caspase-9 activity was determined using a fluorometric method. Each value represents the mean ± SEM from three independent experiments. * Values significantly differ from the respective control, $p < 0.05$.

in brain tumors. Immunoblotting assays further showed that levels of pro-caspase-3 were decreased after honokiol administration (Fig. 6C, first panel, lane 2), and levels of cleaved caspase-3 obviously increased (second panel, lane 2). In addition, administration of honokiol increased protein levels of p-p53, p53, and p21 (Fig. 6D, top three panels, lane 2). As to expression levels of cell cycle-related proteins, levels of CDK6, CDK4, cyclin D1, p-RB, and E2F1 all decreased with honokiol treatment (Fig. 6E, top four and sixth panels, lane 2), whereas the level of the RB protein increased (fifth panel, lane2).

Discussion

Honokiol exerts antiproliferative activity against glioma cells. Our previous study has shown that honokiol can pass through the BBB (Lin et al. 2012). Malignant gliomas are the most aggressive primary brain tumors (Cheng et al. 2012). In this study, we showed that exposure to honokiol induced G_0/G_1 cell cycle arrest and apoptosis which suppressed the growth of human U87 MG or human U373MG glioma cells and prolonged the survival of intracranial glioma-bearing mice. Moreover, honokiol induced U87 MG cell cycle arrest via a p53-dependent signaling pathway. Activation of p53 can promote cell growth arrest when cells are damaged by stimuli (Xu et al. 2011). The CDK inhibitor, p21, is one target of the p53 tumor suppressor and can regulate the G_1-S transition (Niehrs and Acebron 2012). Herein, we showed that exposure to honokiol induced G_0/G_1 cell cycle arrest at 24 ~ 72 h, with upregulation of p-p53, p53, and p21 in glioma cells, and in brain tumor tissues. PFN-α inhibits the p53 protein itself and suppresses transactivation of p53-responsive genes, including cyclin G, *p21/Waf-1*, and *mdm2* (Komarov et al. 1999). In this study, *PFN-α could* reduce the protein level of p21 and diminished cell cycle arrest in U87 MG cells. Therefore, our study proved that honokiol induces p53/p21-mediated cell cycle arrest. However, a study by Lee et al. (2006) showed that p21 can also be induced by a p53-independent pathway. After treatment with honokiol, the p38 mitogen activated protein kinase activates the promoter activity of p21, and consequently causes cell growth inhibition of vascular smooth muscle cells. Therefore, honokiol-induced cell cycle arrest may be either p53-dependent or -independent in different models.

The cell cycle progression from the G_1 to S phase is controlled by CDKs and cyclin complexes. Our data showed that the expressions of CDK6, CDK4, and the cyclin D1 protein were reduced by honokiol *in vitro* and *in vivo*. It was proven that increased p21 inhibits cyclin-CDKs activities by targeting CDKs (Jung et al. 2010). In addition, the p53-inducible protein lessened cyclin D1 transcription in NIH 3T3 cells (Guardavaccaro et al. 2000). Cyclin D1 promoter activity as well as cyclin D1 protein and mRNA levels were suppressed by p53 through downregulating Bcl-3 protein levels and increasing the association of p53 with histone deacetylase 1, resulting in the cell cycle arrest of human non-small-cell lung carcinoma H1299 cells (Rocha et al. 2003). Similar to those studies, our results showed that inhibition of p53 by PFN-α increased honokiol-reduced protein levels of CDK6, CDK4, and cyclin D, suggesting that p53/p21 can regulate cell cycle progression through inhibiting protein expressions of CDKs and cyclin D in honokiol-treated glioma cells.

The RB protein is a key regulator of cell cycle progression. The activity of the RB protein can alter the response of chemotherapeutics, including cisplatin, etoposide, and 5-fluorouracil against human non-small cell lung cancer cell lines (Reed et al. 2007). Loss of the RB protein's function leads to deregulation of cell cycle control and chemosensitivity (Knudsen et al. 2000). Moreover, decreases in phospho- and total-RB proteins were correlated with suppression of E2F1 transcriptional activity in honokiol-treated PC-3 and LNCaP prostate cells (Hahm and Singh 2007). In this study, we also proved that levels of both the p-RB and E2F1 proteins decreased in honokiol-treated glioma cells and brain tumor tissues. Inhibition of p53 reduced honokiol-induced cell cycle arrest and reversed levels of the p-RB and E2F1 proteins. Therefore, honokiol may induce activation of p53, which consequently interferes with the function of the RB and E2F1 proteins which results in glioma cell growth suppression at the G_0/G_1 phase.

The RB protein is phosphorylated by cyclin D-CDK4/6, and is then separated from E2F, which transactivates genes necessary for the G_1/S transition and S phase (Jung et al. 2010). A CDK4/6 inhibitor, LY2835219, inhibits RB phosphorylation resulting in G_1 phase arrest which inhibits proliferation of colorectal cancer and acute myeloid leukemia cells, and inhibits tumor growth in tumor xenografts (Gelbert et al. 2014). Our results also showed deceases in CDK4, CDK6, cyclin D1, and p-RB proteins in honokiol-treated glioma cells, suggesting that honokiol may suppress RB protein phosphorylation via inhibiting CDK4/6. The association of p21 with the cyclin D-CDK4/6 complex inhibits the function of the RB protein (Harbour and Dean 2000). Treatment of HT-29 human colon cancer cells with 3,3′-diindolylmethane increased protein levels of p21 and p27, which decreased levels of cyclin A, D1, CDK4, p-RB, and E2F, resulting in arrest at the G_1 and G_2/M phases (Choi et al. 2009). On the contrary, deficiencies of p53, p21, and/or pRB in hepatocytes diminished transforming growth factor-β-induced cell cycle arrest (Sheahan et al. 2007). In this study, a p53 inhibitor reversed protein levels of CDK4, CDK6, cyclin D1, p-RB, and E2F1 *in vitro* and *in vivo*, demonstrating that CDK-regulated RB phosphorylation is modulated by p53/p21. Therefore, the RB-targeted therapy may be a new strategy for cancer therapy.

Our finding indicates that honokiol can lead to caspase-dependent apoptotic death of glioma cells. Characteristics of apoptosis, including the phosphatidylserine externalization and cleavage of caspase-3 were induced by honokiol. However, honokiol did not induce necrosis. Caspase-8 and -9 are two typical molecules indicating the extrinsic and intrinsic mechanisms of cell apoptosis, respectively (Lavrik and Krammer 2012). Our data showed the major effects of honokiol on augmentation in caspase-9 activities. Thus, honokiol induced apoptosis of human glioma cells mainly through an intrinsic pathway. Previous studies proved that honokiol upregulates expressions of Bax, Bak, and Bad in human prostate cancer cells (Hahm et al. 2008), downregulates expressions of Bid, Bcl-2, or Bcl-xL, and activates caspase cascades in human breast cancer and hepatoma cells (Park et al. 2009). Similarly, our previous study showed that honokiol induces apoptosis of neuroblastoma cells via a Bax-mitochondrion-cytochrome *c*-caspase pathway (Lin et al. 2012). Honokiol could interact with glucose-regulated protein 78 to induce endoplasmic reticulum stress-mediated apoptosis in neuroectodermal tumor cells (Martin et al. 2013). Therefore, honokiol may induce apoptosis of cancer cells though different signaling pathways.

In summary, this study showed that honokiol decreased the viability of U87 MG or U373MG cells though inducing G_0/G_1 cell cycle arrest and caspase-dependent apoptosis. Activation of p53

by honokiol increased its target p21 level and altered protein levels of cell cycle regulators, including CDK6, CDK4, cyclin D1, p-RB, and E2F1. Pharmacologic inhibition of p53 terminates the effect of honokiol-induced growth arrest. In the *in vivo* brain tumor model, honokiol prolonged the survival rate of nude mice with intracranial gliomas through regulating the cell cycle and inducing apoptosis. Taken together, this study showed that honokiol possessed anticancer effects against glioma cells though inducing growth arrest and apoptosis, and prolonged the life of nude mice with intracranial gliomas. Our results provide a strategy for treating patients with malignant gliomas. However, the effects of honokiol at normal or much lower concentrations on angiogenic factors, including hypoxia-induced factors, will be further investigated in our next study.

Conflict of interest

The authors declare no conflicts of interest.

Acknowledgments

This work was supported by grants from Wan-Fang Hospital (105swf04) and the Health and Welfare Surcharge of Tobacco Products (MOHW104-TDU-B-212-124001; MOHW105-TDU-B-212134001), Taipei, Taiwan. The authors appreciate Kelly Huang's skillful technical assistance.

References

Becker, E.B., Bonni, A., 2004. Cell cycle regulation of neuronal apoptosis in development and disease. Prog. Neurobiol. 72, 1–25.

Chen, R.M., Tai, Y.T., Chen, T.G., Lin, T.H., Chang, H.C., Chen, T.L., Wu, G.J., 2013. Propofol protects against nitrosative stress-induced breakage of the blood-brain barrier through reducing apoptotic insults to cerebrovascular endothelial cells. Surgery 154, 58–68.

Cheng, Y., Zhang, Y., Zhang, L., Ren, X., Huber-Keener, K.J., Liu, X., Zhou, L., Liao, J., Keihack, H., Yan, L., Rubin, E., Yang, J.M., 2012. MK-2206, a novel allosteric inhibitor of Akt, synergizes with gefitinib against malignant glioma via modulating both autophagy and apoptosis. Mol. Cancer. Ther. 11, 154–164.

Choi, H.J., Lim do, Y., Park, J.H., 2009. Induction of G1 and G2/M cell cycle arrests by the dietary compound 3,3′-diindolylmethane in HT-29 human colon cancer cells. BMC Gastroenterol 9, 39.

Curtin, J.F., Liu, N., Candolfi, M., Xiong, W., Assi, H., Yagiz, K., Edwards, M.R., Michelsen, K.S., Kroeger, K.M., Liu, C., Muhammad, A.K., Clark, M.C., Arditi, M., Comin-Anduix, B., Ribas, A., Lowenstein, P.R., Castro, M.G., 2009. HMGB1 mediates endogenous TLR2 activation and brain tumor regression. PLoS Med. 6, e10.

Gelbert, L.M., Cai, S., Lin, X., Sanchez-Martinez, C., Del Prado, M., Lallena, M.J., Torres, R., Ajamie, R.T., Wishart, G.N., Flack, R.S., Neubauer, B.L., Young, J., Chan, E.M., Iversen, P., Cronier, D., Kreklau, E., de Dios, A., 2014. Preclinical characterization of the CDK4/6 inhibitor LY2835219: *in-vivo* cell cycle-dependent/independent anti-tumor activities alone/in combination with gemcitabine. Invest. New Drugs 32, 825–837.

Guardavaccaro, D., Corrente, G., Covone, F., Micheli, L., D'Agnano, I., Starace, G., Caruso, M., Tirone, F., 2000. Arrest of G(1)-S progression by the p53-inducible gene PC3 is Rb dependent and relies on the inhibition of cyclin D1 transcription. Mol. Cell Biol. 20, 1797–1815.

Gunther, W., Pawlak, E., Damasceno, R., Arnold, H., Terzis, A.J., 2003. Temozolomide induced apoptosis and senescence in glioma cells cultured as multicellular apheroids. Brit. J. Cancer 88, 463–469.

Hahm, E.R., Arlotti, J.A., Marynowski, S.W., Singh, S.V., 2008. Honokiol, a constituent of oriental medicinal herb magnolia officinalis, inhibits growth of PC-3 xenografts *in vivo* in association with apoptosis induction. Clin. Cancer Res. 14, 1248–1257.

Hahm, E.R., Singh, S.V., 2007. Honokiol causes G0-G1 phase cell cycle arrest in human prostate cancer cells in association with suppression of retinoblastoma protein level/phosphorylation and inhibition of E2F1 transcriptional activity. Mol. Cancer Ther. 6, 2686–2695.

Harbour, J.W., Dean, D.C., 2000. The Rb/E2F pathway: expanding roles and emerging paradigms. Genes Dev. 14, 2393–2409.

Ishikawa, C., Arbiser, J.L., Mori, N., 2012. Honokiol induces cell cycle arrest and apoptosis via inhibition of survival signals in adult T-cell leukemia. Biochim. Biophys. Acta 1820, 879–887.

Jung, Y.S., Qian, Y., Chen, X., 2010. Examination of the expanding pathways for the regulation of p21 expression and activity. Cell Signal 22, 1003–1012.

Knudsen, K.E., Booth, D., Naderi, S., Sever-Chroneos, Z., Fribourg, A.F., Hunton, I.C., Feramisco, J.R., Wang, J.Y., Knudsen, E.S., 2000. RB-dependent S-phase response to DNA damage. Mol. Cell Biol. 20, 7751–7763.

Komarov, P.G., Komarova, E.A., Kondratov, R.V., Christov-Tselkov, K., Coon, J.S., Chernov, M.V., Gudkov, A.V., 1999. A chemical inhibitor of p53 that protects mice from the side effects of cancer therapy. Science 285, 1733–1737.

Lavrik, I.N., Krammer, P.H., 2012. Regulation of CD95/Fas signaling at the DISC. Cell Death Differ. 19, 36–41.

Lee, B., Kim, C.H., Moon, S.K., 2006. Honokiol causes the p21WAF1-mediated G(1)-phase arrest of the cell cycle through inducing p38 mitogen activated protein kinase in vascular smooth muscle cells. FEBS Lett. 580, 5177–5184.

Lin, J.W., Chen, J.T., Hong, C.Y., Lin, Y.L., Wang, K.T., Yao, C.J., Lai, G.M., Chen, R.M., 2012. Honokiol traverses the blood-brain barrier and induces apoptosis of neuroblastoma cells via an intrinsic bax-mitochondrion-cytochrome c-caspase protease pathway. Neuro-Oncol. 14, 302–314.

Liu, T.G., Xiong, S.Q., Yan, Y., Zhu, H., Yi, C., 2012. Use of Chinese herb medicine in cancer patients: a survey in southwestern china. Evid. Based Complement Alternat. Med. 2012, 769042.

Martin, S., Lamb, H.K., Brady, C., Lefkove, B., Bonner, M.Y., Thompson, P., Lovat, P.E., Arbiser, J.L., Hawkins, A.R., Redfern, C.P., 2013. Inducing apoptosis of cancer cells using small-molecule plant compounds that bind to GRP78. Br. J. Cancer 109, 433–443.

Nagalingam, A., Arbiser, J.L., Bonner, M.Y., Saxena, N.K., Sharma, D., 2012. Honokiol activates AMP-activated protein kinase in breast cancer cells via an LKB1-dependent pathway and inhibits breast carcinogenesis. Breast Cancer Res. 14, R35.

Niehrs, C., Acebron, S.P., 2012. Mitotic and mitogenic Wnt signalling. EMBO J. 31, 2705–2713.

Park, E.J., Min, H.Y., Chung, H.J, Hong, J.Y., Kang, Y.J., Hung, T.M., Youn, U.J., Kim, Y.S., Bae, K., Kang, S.S., Lee, S.K., 2009. Down-regulation of c-Src/EGFR-mediated signaling activation is involved in the honokiol-induced cell cycle arrest and apoptosis in MDA-MB-231 human breast cancer cells. Cancer Lett. 277, 133–140.

Pietra, G., Mortarini, R., Parmiani, G., Anichini, A., 2001. Phases of apoptosis of melanoma cells, but not of normal melanocytes, differently affect maturation of myeloid dendritic cells. Cancer Res. 61, 8218–8226.

Reed, M.F., Zagorski, W.A., Knudsen, E.S., 2007. RB activity alters checkpoint response and chemosensitivity in lung cancer lines. J. Surg. Res. 142, 364–372.

Rocha, S., Martin, A.M., Meek, D.W., Perkins, N.D., 2003. p53 represses cyclin D1 transcription through down regulation of Bcl-3 and inducing increased association of the p52 NF-kappaB subunit with histone deacetylase 1. Mol. Cell Biol. 23, 4713–4727.

Sheahan, S., Bellamy, C.O., Dunbar, D.R., Harrison, D.J., Prost, S., 2007. Deficiency of G1 regulators P53, P21Cip1 and/or pRb decreases hepatocyte sensitivity to TGF-β cell cycle arrest. BMC Cancer 7, 215.

Staudacher, I., Jehle, J., Staudacher, K., Pledl, H.W., Lemke, D., Schweizer, P.A., Becker, R., Katus, H.A., Thomas, D., 2014. HERG K+ channel-dependent apoptosis and cell cycle arrest in human glioblastoma cells. PLoS One 9, e88164.

Stupp, R., Mason, W.P., van den Bent, M.J., et al., 2005. Radiotherapy plus concomitant and adjuvant temozolomide for glioblastoma. N. Engl. J. Med. 352, 987–996.

Tan, W., Lu, J., Huang, M., Li, Y., Chen, M., Wu, G., Gong, J., Zhong, Z., Xu, Z., Dang, Y., Guo, J., Chen, X., Wang, Y., 2011. Anti-cancer natural products isolated from Chinese medicinal herbs. Chin. Med. 6, 27.

Wang, X., Duan, X., Yang, G., Zhang, X., Deng, L., Zheng, H., Deng, C., Wen, J., Wang, N., Peng, C., Zhao, X., Wei, Y., Chen, L., 2011. Honokiol crosses BBB and BCSFB, and inhibits brain tumor growth in rat 9 L intracerebral gliosarcoma model and human U251 xenograft glioma model. PLoS One 6, e18490.

Xu, H.L., Tang, W., Du, G.H., Kokudo, N., 2011. Targeting apoptosis pathways in cancer with magnolol and honokiol, bioactive constituents of the bark of Magnolia officinalis. Drug Discov. Ther. 5, 202–510.